ELSEVIER

Materials Science and Engineering A 416 (2006) 18–32

MATERIALS SCIENCE & ENGINEERING A

www.elsevier.com/locate/msea

In situ investigation of the crystallization kinetics and the mechanism of grain refinement in aluminum alloys

N. Iqbal [a,*], N.H. van Dijk [a], S.E. Offerman [b], N. Geerlofs [b], M.P. Moret [c], L. Katgerman [b], G.J. Kearley [a]

[a] *Fundamental Aspects of Materials and Energy, Faculty of Applied Sciences, Delft University of Technology, Mekelweg 15, 2629 JB Delft, The Netherlands*

[b] *Department of Materials Science and Engineering, Delft University of Technology, Rotterdamseweg 137, 2628 AL Delft, The Netherlands*

[c] *European Synchrotron Radiation Facility, 6 Rue Jules Horowitz, BP 220, 38043 Grenoble Cedex 9, France*

Received in revised form 1 August 2005; accepted 1 October 2005

Abstract

The crystallization kinetics during the liquid to solid phase transformation of pure aluminium and various Al–Ti–B alloys is investigated using differential thermal analysis (DTA) and three-dimensional X-ray diffraction (3D XRD). A reduced undercooling required to activate nucleation of aluminum grains is observed, when both solute titanium and TiB_2 particles are present in the liquid. The cooling rate dependence of the onset temperature T_o, the crystallization peak temperature T_p, and the latent heat ΔH are evaluated and compared for all samples. The DTA curves for slow cooling of an Al–0.3Ti–0.02B (wt.%) alloy illustrate the formation of an aluminide phase ($TiAl_3$) upon solidification. A comparison of the DTA curves during slow cooling of the hypoperitectic Al–0.1Ti–0.1TiB_2 (wt.%) and the hyperperitectic Al–0.3Ti–0.02B (wt.%) alloys seem to exhibit a kinetic similarity at the onset of the solidification. In situ 3D XRD measurements clearly exhibit the formation of a metastable $TiAl_3$ phase prior to solidification of both alloys. This explains the mechanism of grain refinement in the presence of solute titanium and TiB_2 particles in the grain refined aluminum alloys. The influence of titanium diffusion, latent heat, and cooling rate on the growth behaviour of individual aluminium grains during the phase transformation is further quantified.

Keywords: Synchrotron; Nucleation; Aluminum alloy; Kinetics; DTA

1. Introduction

Grain refinement plays an important role in the liquid to solid phase transformation of aluminum alloys [1,2]. Generally Al–Ti–B master alloys are added to the aluminum alloys to refine the grain size of the solidified product. These alloys contain microscopic TiB_2 and $TiAl_3$ nucleating particles. Although various theories regarding the grain refining mechanisms are proposed [3–8] (e.g. the particle theory, the phase diagram theory, the duplex nucleation theory, and the peritectic hulk theory), the mechanism of grain refinement remains a problem of considerable controversy in the scientific literature. The nucleant effects, i.e. which particle nucleates α-Al grains and what are its characteristics, has been the subject of intensive research. Lately, the solute effects, i.e. the effect of dissolved titanium on grain refinement, has come into the forefront of grain refinement research. Therefore, a great interest exists to determine the kinetics of the liquid to solid phase transformation of aluminum alloys in situ in order to determine the role of the microscopic grain refining particles and the solute titanium.

The present paper describes differential thermal analysis (DTA) and three-dimensional X-ray diffraction (3D XRD) measurements on high purity aluminum, Al–0.15TiB_2, Al–0.1Ti, Al–0.1Ti–0.1TiB_2 (wt.%) alloys, and a commercial purity Al–0.3Ti–0.02B (wt.%) alloy during solidification at different cooling rates. The aim of these experiments is to ascertain the mechanisms responsible for grain nucleation and growth and to separate the effects of nucleating particles from that of the solute titanium. Part of the 3D XRD results for the high-purity alloys has been presented previously [9]. These results are also included in the present paper to allow for a systematic comparison of the DTA and 3D XRD data for different cooling rates.

* Corresponding author. Tel.: +31 15 278 4533; fax: +31 15 278 8303.
E-mail address: n.iqbal@tnw.tudelft.nl (N. Iqbal).

0921-5093/$ – see front matter © 2005 Elsevier B.V. All rights reserved.
doi:10.1016/j.msea.2005.10.045

2. Sample preparation

The studied samples were laboratory prepared from high purity aluminum, titanium, and TiB_2 particles. The pure aluminum (99.999%) and titanium (99.99%) were purchased from Goodfellow. The TiB_2 (99.99%) powder with a particle size distribution ranging from 3 to 6 μm and a maximum around 4.4 μm was purchased from Advanced Ceramics.

The Al–0.15TiB_2 (wt.%) alloy was prepared by melting together aluminum lumps with a total mass of 35 g and the TiB_2 particles into an aluminum oxide crucible. The sample was heated to a temperature of T = 1023 K. After holding at this temperature for 30 min, the crucible was removed from the furnace and the liquid alloy was homogenized by stirring using an aluminum oxide rod. After solidification the sample was remelted and the above-mentioned process was repeated three times to ensure that the TiB_2 particles were homogeneously distributed in the Al–0.15TiB_2 (wt.%) alloy.

In order to prepare the Al–0.1Ti (wt.%) alloy, a different route was adopted. First, Al–1Ti (wt.%) master alloy samples, of 5 g each, were prepared by melting together the appropriate amounts of aluminum and titanium in an electric arc furnace in a high purity argon atmosphere. The molten samples were stirred by using the arc flame for homogenization. Then the samples were solidified, rotated by changing the top and bottom positions, and remelted. This process was repeated five times to ensure that titanium is homogeneously distributed in the sample. Having prepared the Al–1Ti (wt.%) master alloy, the Al–0.1Ti and Al–0.1Ti–0.1TiB_2 (wt.%) samples were prepared by melting the master alloy together with an appropriate amount of high purity aluminum and TiB_2 particles, by the method described for the Al–0.15TiB_2 sample. The chemical composition of these aluminum alloys was confirmed by X-ray fluorescence spectroscopy (XRF).

The Al–0.3Ti–0.02B (wt.%) alloy was prepared from an Al–5Ti–0.2B (wt.%) commercial master alloy (KBM AFFILIPS). The particle size distribution of TiB_2 particles in the Al–0.3Ti–0.02B alloy was determined by optical microscopy and showed a particle size distribution in the range from 0.6 to 2.2 μm with a maximum around 1.2 μm. The chemical composition of this commercial Al–0.3Ti–0.02B alloy was analyzed. It was observed that iron was the main impurity in this alloy with about 0.2 wt.% Fe.

3. Experimental methods

3.1. Differential thermal analysis (DTA)

A Perkin-Elmer DTA instrument was used for measuring the crystallization kinetics during continuous cooling and heating. The instrument was calibrated using high purity zinc and aluminum samples for each of the applied cooling rates used in the measurements. All measurements were carried out in a helium atmosphere. From all alloys, solid samples with a cubic shape and with dimensions of 2 mm × 2 mm × 2 mm were used. For the crystallization experiment, the samples were heated to 973 K and kept for 5 min at that temperature to ensure that the sample is completely molten. Then the samples were cooled at constant rates of 0.5, 1, 5, 10, and 20 K/min. The exothermic crystallization peak was recorded as a function of temperature. In order to investigate the corresponding melting behaviour, a sample of each material composition was also heated with a heating rate of 10 K/min. The corresponding endothermic peak was recorded as a function of temperature.

3.2. Three-dimensional X-ray diffraction (3D XRD)

In order to resolve the nucleation process from the subsequent grain growth, in situ X-ray diffraction measurements were performed on the three-dimensional X-ray diffraction (3D XRD) microscope at the ID11 beam line at the European synchrotron radiation facility (ESRF). A monochromatic beam of hard X-rays with an energy of 70 keV illuminated each sample. The samples were placed in a glassy carbon container with a height of 20 mm, an inner diameter of 5 mm, and a wall thickness of 1 mm. The sample container was then placed into a quartz tube that was part of the vacuum furnace. A small sample rotation around an axis perpendicular to the beam gives rise to a diffraction pattern on the two-dimensional detector that is placed behind the sample. For a small illuminated sample volume, the diffraction spots originating from solid aluminium grains in the liquid metal do not form continuous powder diffraction rings, but instead appear as distinct spots on the two-dimensional detector during solidification. The measuring procedure aimed to determine the nucleation rate by measuring the number of diffraction spots on the detector as a function of time during solidification. The intensity change of these diffraction spots is a measure of the grain volume. The solidification experiments involved continuous cooling of molten samples, held at 973 K for 30 min, at different cooling rates. The complete details of the experimental setup and measuring procedure are given elsewhere [10].

4. Results and discussion

4.1. DTA measurements

4.1.1. Crystallization behaviour

Fig. 1 shows the typical DTA curves obtained for pure aluminum, Al–0.15TiB_2, Al–0.1Ti, Al–0.1Ti–0.1TiB_2, and Al–0.3Ti–0.02B (wt.%) alloys during solidification at a constant cooling rate of 20 K/min. Two characteristic phenomena are resolved in the studied temperature range at this cooling rate. The first one corresponds to the variation in onset temperature of crystallization (T_o) and the second to the peak temperature of crystallization (T_P).

A complete set of DTA thermograms, measured for all sample compositions and at different cooling rates from 0.5 to 10 K/min is shown in Fig. 2. It is clear that the exothermic curves become wider and the characteristic temperatures shift to the lower values as the cooling rate increases. Table 1 summarizes the characteristic data of the crystallization exotherms for all the samples studied. The undercooling is maximum for pure aluminium. A relatively low undercooling is found to activate the nucleation of aluminum grains upon solidification when both

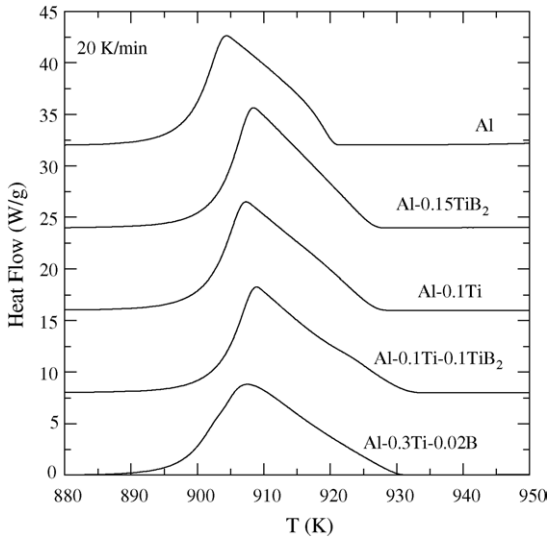

Fig. 1. Crystallization curves of the liquid to solid phase transformation for pure aluminum, Al–0.15TiB_2, Al–0.1Ti, Al–0.1Ti–0.1TiB_2, and Al–0.3Ti–0.02B alloys at a cooling rate of 20 K/min (for clarity each curve is shifted from the previous one by adding eight).

solute titanium and TiB_2 particles are present, as observed for the Al–0.1Ti–0.1TiB_2 and Al–0.3Ti–0.02B alloys. A higher undercooling is observed during solidification of the Al–0.15TiB_2 alloy, which confirms the poor surface properties of the TiB_2 particles to activate the nucleation of solid aluminium in the absence of solute titanium.

The question of fundamental interest is how a small amount of titanium enhances the nucleation efficiency of the TiB_2 particles. From the curves shown in Fig. 2, it is apparent that the DTA exotherms for the Al–0.3Ti–0.02B (wt.%) sample exhibit distinct peaks upon freezing at a temperature above ($T > T_P$), and below ($T < T_P$) the crystallization peak temperature, with a size and shape that depends on the cooling rate. Calculations using the thermodynamic database MTDATA suggest that the two additional peaks observed in the commercial purity Al–0.3Ti–0.02B sample, predominantly at low cooling rates, correspond to the formation of $TiAl_3$ (for $T > T_P$) and Fe_4Al_{13} (for $T < T_P$).

The formation of a $TiAl_3$ phase in the hyperperitectic Al–0.3Ti–0.02B alloy favours an enhanced nucleation in this sample. The experimental results of Mohanty and Gruzleski [11] and Schumacher and Greer [12] have suggested that $TiAl_3$ lay-

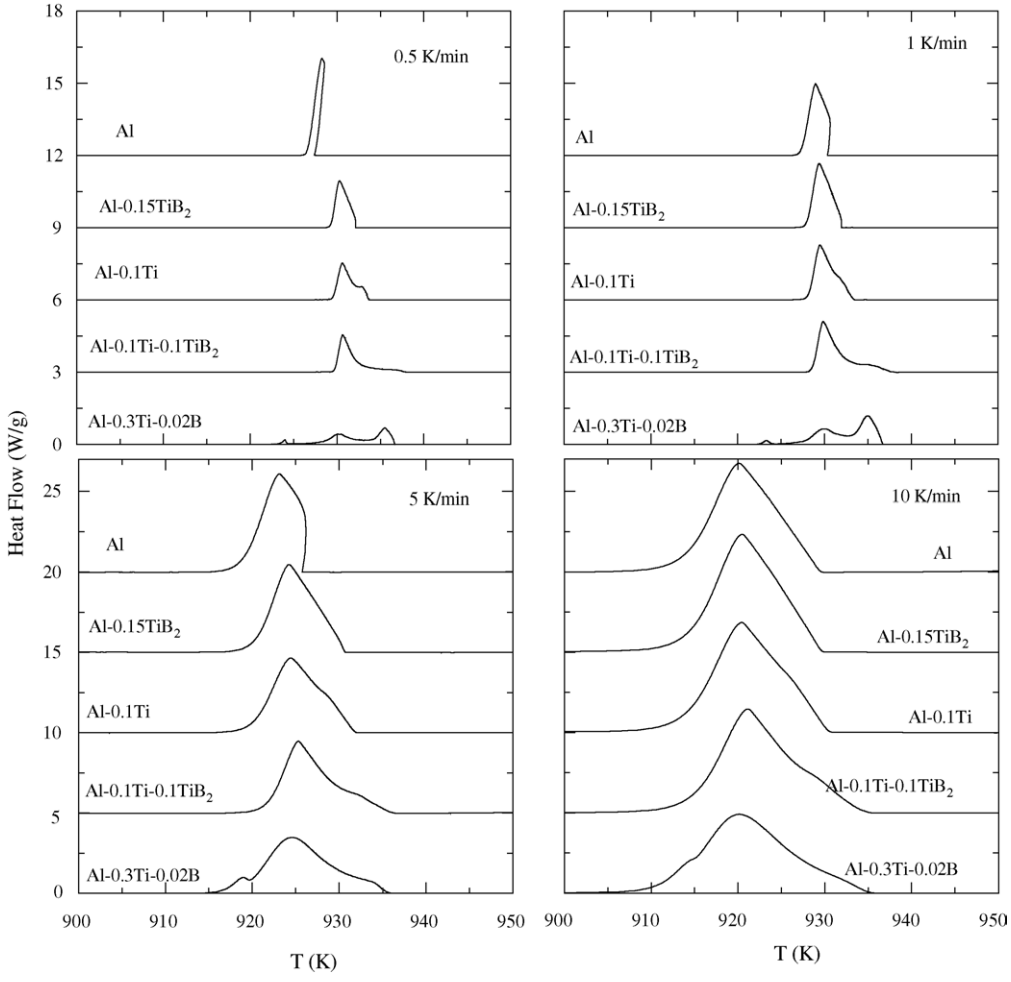

Fig. 2. Crystallization curves of the liquid to solid phase transformation at pure aluminum, Al–0.15TiB_2, Al–0.1Ti, Al–0.1Ti–0.1TiB_2 and Al–0.3Ti–0.02B alloys for cooling rates of 0.5, 1, 5, and 10 K/min (for clarity each curve for 0.5 and 1 K/min is shifted by adding three while for 5 and 10 K/min is shifted by adding five).

Table 1
Characteristic temperatures T_{on} and T_p and the heat released ΔH for the crystallization of aluminum alloys during continuous cooling at different cooling rates

	Cooling rate (K/min)				
	0.5	1.0	5.0	10.0	20.0
Al					
T_{on} (K)	927.5	930.4	925.8	929.4	922.8
T_p (K)	928.3	928.9	923.1	920.1	912.3
ΔH (J/g)	426	423	381	349	404
Al–0.15TiB_2					
T_{on} (K)	932.1	931.9	930.6	929.6	927.5
T_p (K)	930.2	929.4	924.2	920.5	913.2
ΔH (J/g)	426	422	386	373	435
Al–0.1Ti					
T_{on} (K)	933.6	933.5	931.8	930.4	928.0
T_p (K)	930.6	929.5	924.4	920.4	912.9
ΔH (J/g)	405	404	373	364	423
Al–0.1Ti–0.1TiB_2					
T_{on} (K)	937.8	938.3	936.7	935.3	933.3
T_p (K)	930.7	929.8	925.3	921.2	913.7
ΔH (J/g)	409	421	374	364	425
Al–0.3Ti–0.02B					
T_{on} (K)	936.6	936.7	935.6	935.1	931.9
T_p (K)	930.0	929.4	924.7	920.2	913.0
ΔH (J/g)	438	348	384	343	426

The value of latent heat reported for pure aluminum is 385 J/g [18].

ers are formed on the surface of TiB_2 particles. Thus, $TiAl_3$, due to its better lattice compatibility with solid aluminium, makes it an efficient nucleation site for aluminum grains upon solidification. A comparison of DTA curves during solidification of the Al–0.1Ti–0.1TiB_2 and Al–0.3Ti–0.02B alloys seems to exhibit a kinetic similarity and close resemblance in the required undercooling before solidification. This similarity in freezing behaviour suggests that the same nucleation mechanism, through the formation of $TiAl_3$ phase, might be responsible for the enhanced nucleation during grain refinement in hypoperitectic Al–0.1Ti–0.1TiB_2 alloy, as observed for the Al–0.3Ti–0.02B alloy.

A phenomenological asymmetry is observed at the right- and left-hand side of the DTA curves during the liquid to solid phase transformation. During slow cooling of pure aluminum the peak temperature of exothermal curve is even higher than the onset temperature. This indicates that the exothermal rate, due to the release of latent heat in the sample, during freezing is larger than the heat removal due to slow cooling. The reference crucible is placed in the neighbourhood of sample, and there is significant heat flux probable from the sample to reference crucible. This elevates the reference temperature, which is plotted in horizontal axis of DTA curves. At the beginning of the solidification, the exothermal rate seems to decrease with the addition of solute titanium, which in fact reduces the growth of aluminum grains and hence the solid fraction. When both solute titanium and TiB_2 particles are present, then in addition to a growth reduction, the nucleation starts at a relatively low undercooling as shown in Fig. 2. The variation in slope at the right-hand side of the DTA curves might be associated with the variation in nucleation behaviour caused by the release of latent heat. As the nucleation rate strongly increases with the melt undercooling, a slight decrease in melt undercooling, e.g. due to the release of latent heat, can abruptly cease the nucleation process. After the onset of the solidification the evolution of the solid fraction is controlled by both nucleation and growth. Soon after the nucleation starts, the release of latent heat stops the nucleation process. Finally, the solid fraction is controlled only by grain growth.

The difference in crystallization kinetics for the different investigated samples during solidification can also be analysed by comparing the relative crystallinity as a function of temperature $X(T)$ deduced directly from the heat flow (dH_C/dT) by using

$$X(T) = \frac{\int_{T_o}^{T} (dH_C/dT)\,dT}{\int_{T_o}^{T_\infty} (dH_C/dT)\,dT} \quad (1)$$

where T_o and T_∞ represent the crystallization onset temperature and end temperature, respectively. H_C is the enthalpy of crystallization. Fig. 3 shows the relative degree of crystallinity $X(T)$, as a function of temperature for all the high purity samples studied at various cooling rates. The crystallization curves exhibit the traditional sigmoidal shape for the liquid to solid phase transformation. The transition temperature and transition rate changes significantly with cooling rate and sample composition. Fig. 4 shows the evolution of the relative crystallinity $X(T)$ as a function of temperature during solidification for the commercial purity Al–0.3Ti–0.02B alloy. The results indicate that for higher cooling rates, the crystallization curves are analogous to those in Fig. 3 but change a lot for slow cooling. During slow cooling of the Al–0.3Ti–0.02B alloy, the freezing behaviour is altered by the segregation of titanium and iron present in the melt.

The plots of the relative crystallinity as a function of time $X(T)$ for all the samples at a cooling rate of 10 K/min are illustrated in Fig. 5. It is clear from the plots that for the same cooling rate, the time evolution of the crystallization process during the liquid to solid phase transformation of pure aluminum and Al–0.1TiB_2 is almost identical. The nucleation starts earlier in time, at low undercooling, when both TiB_2 nucleating particles and the solute titanium is present as observed in the Al–0.1Ti–0.1TiB_2 and Al–0.3Ti–0.02B alloys. The addition of solute titanium, even at a hypoperitectic composition, enhances the nucleation potential of TiB_2 grain refining particles as illustrated by the Al–0.1Ti–0.1TiB_2 crystallization curve.

4.1.2. Melting behaviour

In order to investigate the effects of grain refining particles on the melting behaviour of aluminum, the samples were also heated with a constant heating rate of 10 K/min. An example of the endothermic curves and the corresponding change in crystallization fraction with temperature is shown in Fig. 6. The temperature range was chosen to be sufficiently wide to ensure that the melting was complete. The values of the heat absorbed during melting are given in Table 2 for each sample. The experimental results, for the variation in crystal fraction with temperature, for pure aluminum and the TiB_2 particles

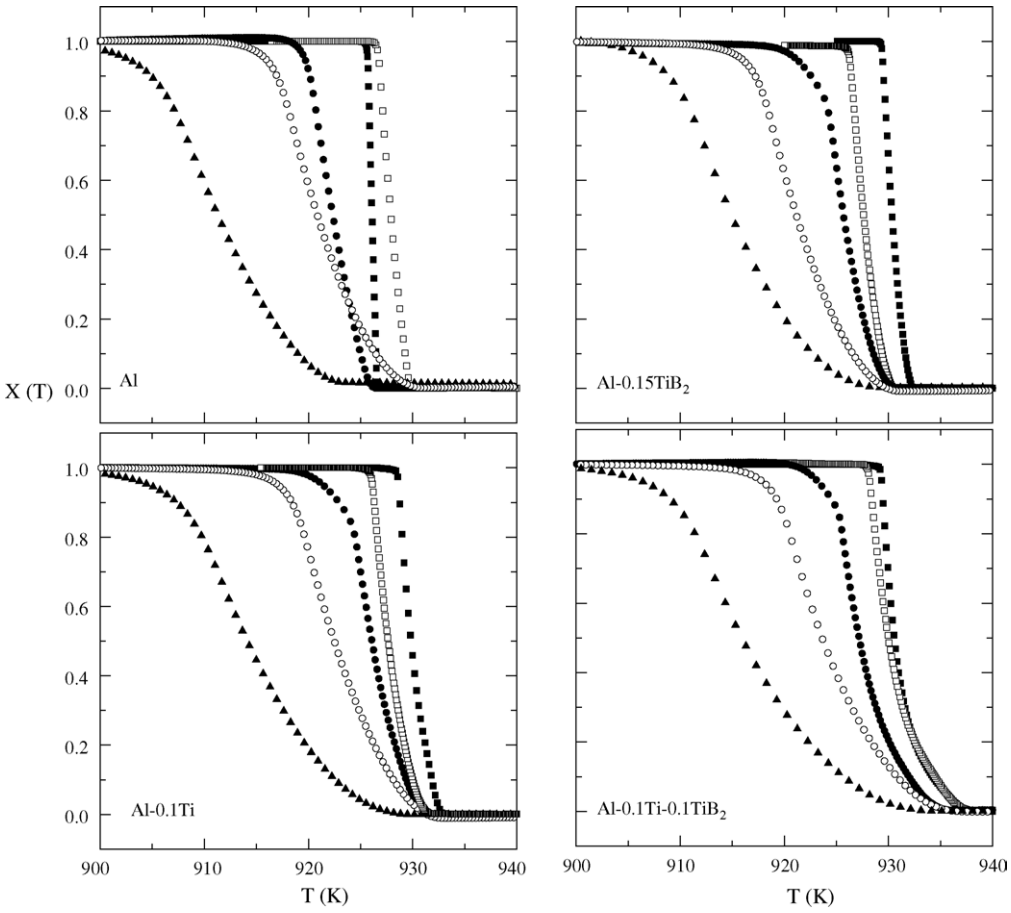

Fig. 3. Relative crystallinity $X(T)$ as a function of temperature for pure aluminum, Al–0.15TiB_2, Al–0.1Ti, and Al–0.1Ti–0.1TiB_2 alloys at a cooling rate of (■) 0.5 K/min, (□) 1 K/min, (●) 5 K/min, (○) 10 K/min, and (▲) 20 K/min cooling rates.

embedded in an Al matrix (Al–0.15TiB_2 alloy) indicate that the presence of TiB_2 impurities does not significantly change the melting kinetics in Al–0.15TiB_2 sample, compared to pure aluminum. The presence of solute titanium in aluminum, as observed in Al–0.1Ti alloy, is found to make a slight change compared to pure aluminum. The presence of Fe_4Al_{13} due to the iron impurities in the commercial purity Al–0.3Ti–0.02B alloy constitutes a needle-like second phase particles with a low melting point. By using optical microscopy, these particles were

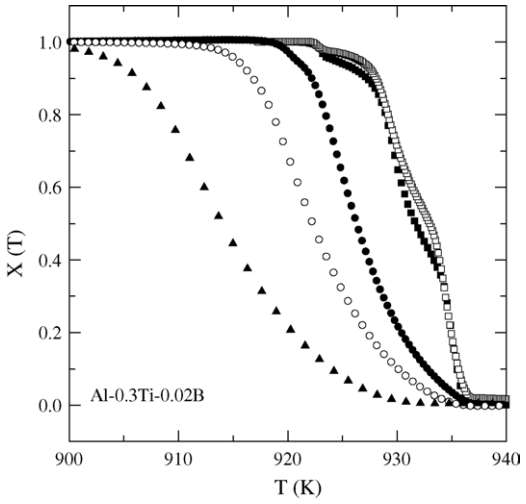

Fig. 4. Relative crystallinity $X(T)$ as a function of temperature for the Al–0.3Ti–0.02B alloy at a cooling rate of (■) 0.5 K/min, (□) 1 K/min, (●) 5 K/min, (○) 10 K/min, and (▲) 20 K/min.

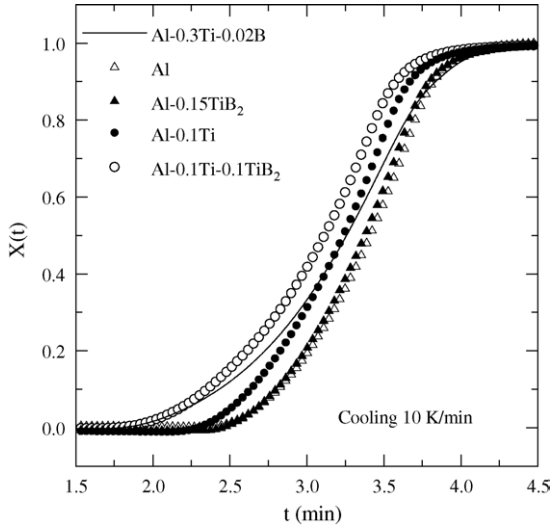

Fig. 5. Relative crystallinity $X(T)$ as a function of time for pure aluminum, Al–0.15TiB_2, Al–0.1Ti, Al–0.1Ti–0.1TiB_2, and Al–0.3Ti–0.02B alloys at a cooling rate of 10 K/min.

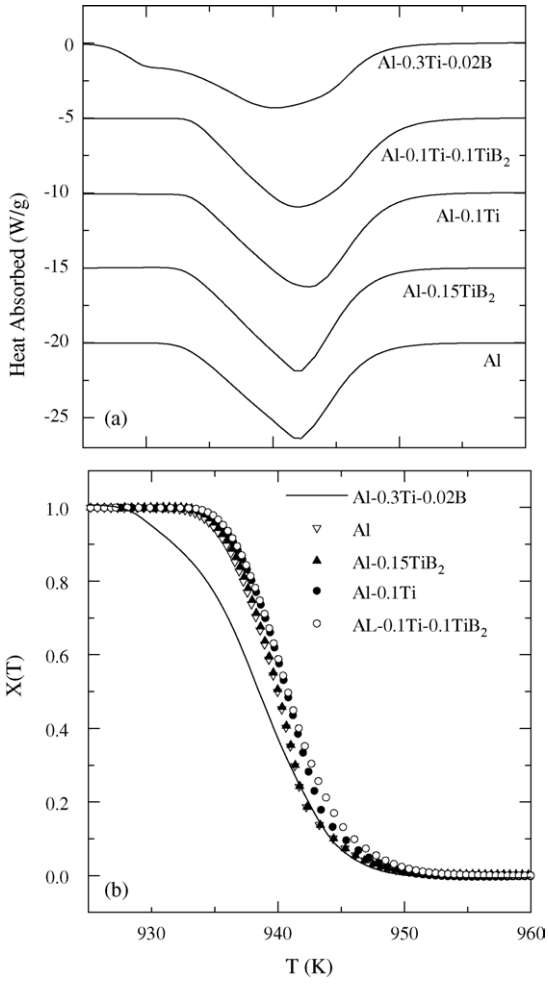

Fig. 6. (a) Crystallization curves for pure aluminum, Al–0.15TiB_2, Al–0.1Ti, Al–0.1Ti–0.1TiB_2 and Al–0.3Ti–0.02B alloys (for clarity each curve is shifted from the previous one by subtracting five) and (b) relative crystallinity as a function of temperature for a heating rate of 10 K/min during melting.

found to be distributed along the grain boundaries, as shown in Fig. 7. The melting of Fe_4Al_{13} starts earlier and hence results in a significant decrease in melting point of the investigated commercial purity sample, as observed in Fig. 6(b).

Fig. 8 illustrates a phenomenological symmetry during melting and freezing of the Al–0.3Ti–0.02B alloy. The melting/freezing transition exhibits a thermal hysteresis and confirms the first order character of phase transformation. The width $\Delta T_{1/2}$ of the transformed fraction $X(T)$ versus T at $X(T) = 0.5$ is a useful quantitative measure of the thermal hysteresis. The corresponding values of $\Delta T_{1/2}$ for all the samples at a cooling/heating rate of 10 K/min are listed in Table 2 and decreases with the addition of grain refiners in aluminum. A comparison of the freezing

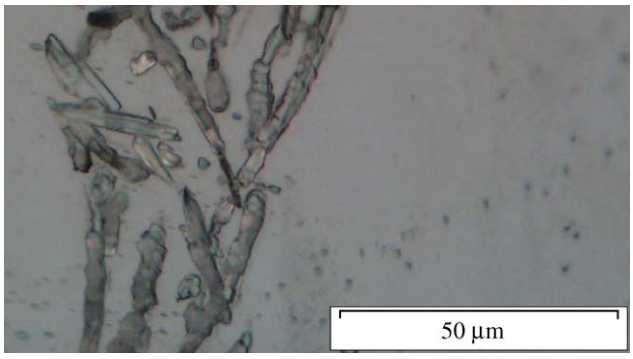

Fig. 7. Optical microscopy image of the commercial purity Al–0.3Ti–0.02B (wt.%) alloy, at the room temperature. The needles like particles are observed at the grain boundary and correspond to the Fe_4Al_{13} phase, formed during solidification.

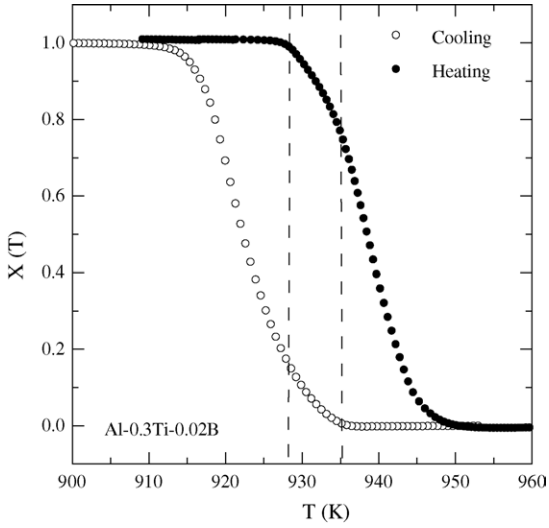

Fig. 8. Temperature dependence of the relative crystallinity for the Al–0.3Ti–0.02B alloy as a function of temperature during cooling and heating for a rate of 10 K/min. (The broken lines indicate the onset of freezing at $T = 935.1$ K and melting at $T = 928.5$ K.)

curves with the equilibrium solidification temperature of aluminum (broken line at $T = 933$ K) in Fig. 9, clearly demonstrates the presence of significant undercooling during solidification of pure aluminum and Al–0.15TiB_2 alloys, while almost no undercooling is observed for Al–0.1Ti and Al–0.1Ti–0.1TiB_2 alloys.

4.2. Grain nucleation and growth studied by 3D XRD

In order to quantify the grain nucleation and growth behaviour of individual aluminium grains during solidification of these

Table 2
Heat absorbed ΔH during melting of aluminum alloys for a heating rate of 10 K/min, and the corresponding melting/freezing transformation width $\Delta T_{1/2}$

	Sample				
	Al	Al–0.15TiB_2	Al–0.1Ti	Al–0.1Ti–0.1TiB_2	Al–0.3Ti–0.02B
$\Delta T_{1/2}$ (K)	19.1	18.8	18.3	17.2	16.1
ΔH (J/g)	339	361	350	375	317

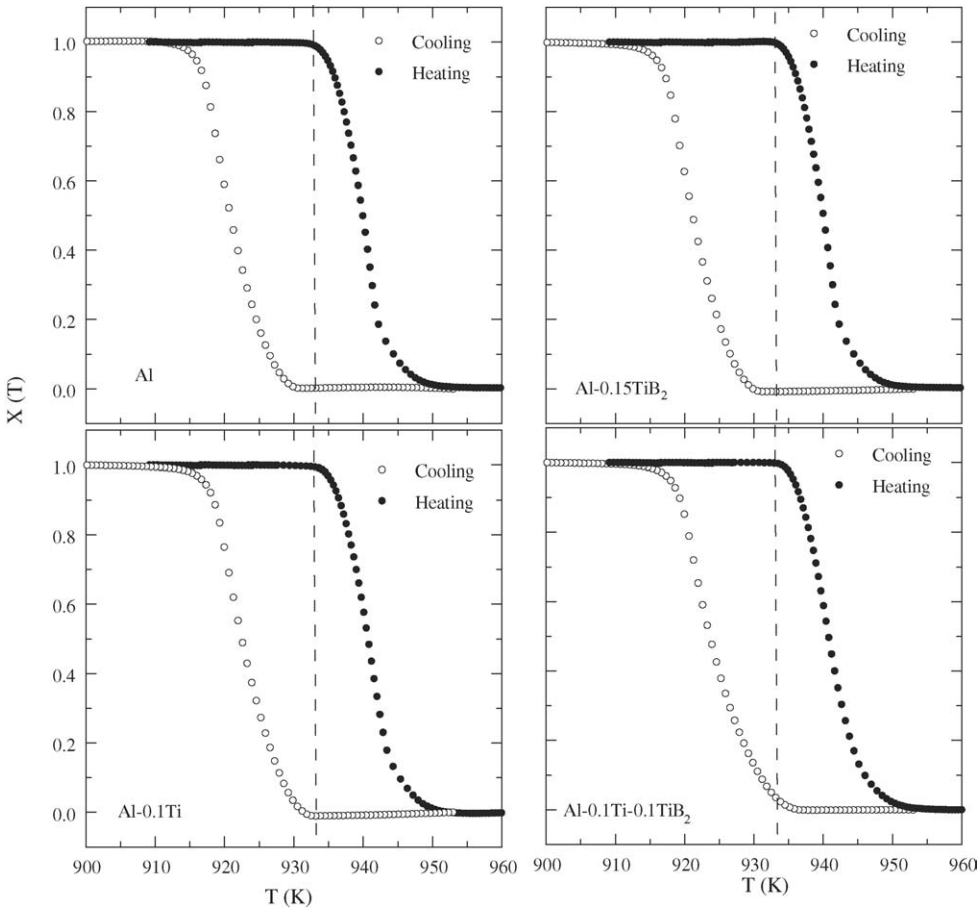

Fig. 9. Temperature dependence of the relative crystallinity for pure aluminum, Al–0.15TiB_2, Al–0.1Ti and Al–0.1Ti–0.1TiB_2 alloys as a function of temperature during cooling and heating for a rate of 10 K/min. (The broken line indicates the solidification temperature of pure aluminum at $T = 933$ K.)

samples, three-dimensional X-ray diffraction measurements were performed. The experimental results describing the nucleation and growth of individual aluminium grains during solidification, with two different cooling rates at 1 and 10 K/min, of high purity grain refined Al–Ti–B alloys have been previously reported in [9]. The experimental findings with these model alloys have provided evidence for the formation of a long debated metastable $TiAl_3$ phase, responsible for grain refinement in hypoperitectic grain refined aluminium titanium alloy. This article presents a detailed study of 3D XRD measurements during solidification of model alloys and compares the results with a commercial purity sample with hyperperitectic composition. As expected [1,2], the formation of $TiAl_3$ phase, prior to nucleation of aluminium grains in the commercial purity hyperperitectic sample is confirmed during slow cooling. This comparison provides the experimental evidence that $TiAl_3$ is essential nucleation site for grain refinement in hypoperitectic as well as hyperperitectic grain refined aluminium titanium alloy. As cooling rate constitutes an important parameter during solidification. Therefore in addition to the previously reported 3D XRD measurements for model alloys during solidification [9], the detailed results for cooling rates ranging from 1 to 40 K/min are presented. This elaborates the systematic variation of undercooling with cooling rate and consequently its effect on nucleation and grain growth process.

4.2.1. Grain nucleation

For illustration, raw images acquired during the liquid to solid phase transformation of Al–0.1Ti–0.1TiB_2 alloy with a cooling rate of 20 K/min are shown in Fig. 10. The illumination time for each displayed diffraction pattern is 1 s using a beam size of 300 μm × 300 μm and the real time interval between consecutive diffraction patterns is 14 s. The diffraction pattern from the molten sample (a) displays the two characteristic liquid rings associated with the short-range order in the molten aluminum. The inner most ring is due to the scattering from the glassy structure of the quartz tube. The amount of grain refiners present in the aluminum is found to be too small to make a significant change in the short-range order of the molten aluminum. The subsequent diffraction patterns during cooling comprises of diffraction spots from aluminum grains, which nucleate in the beginning and grow till virtually no intensity is left in the liquid rings, indicating that the phase transformation is complete.

The nucleation rate, the corresponding evolution of total number of aluminum grains along with the solid fraction f_S, estimated from the normalized variation in the first liquid peak intensity, during solidification of Al–0.15TiB_2, Al–0.1Ti,

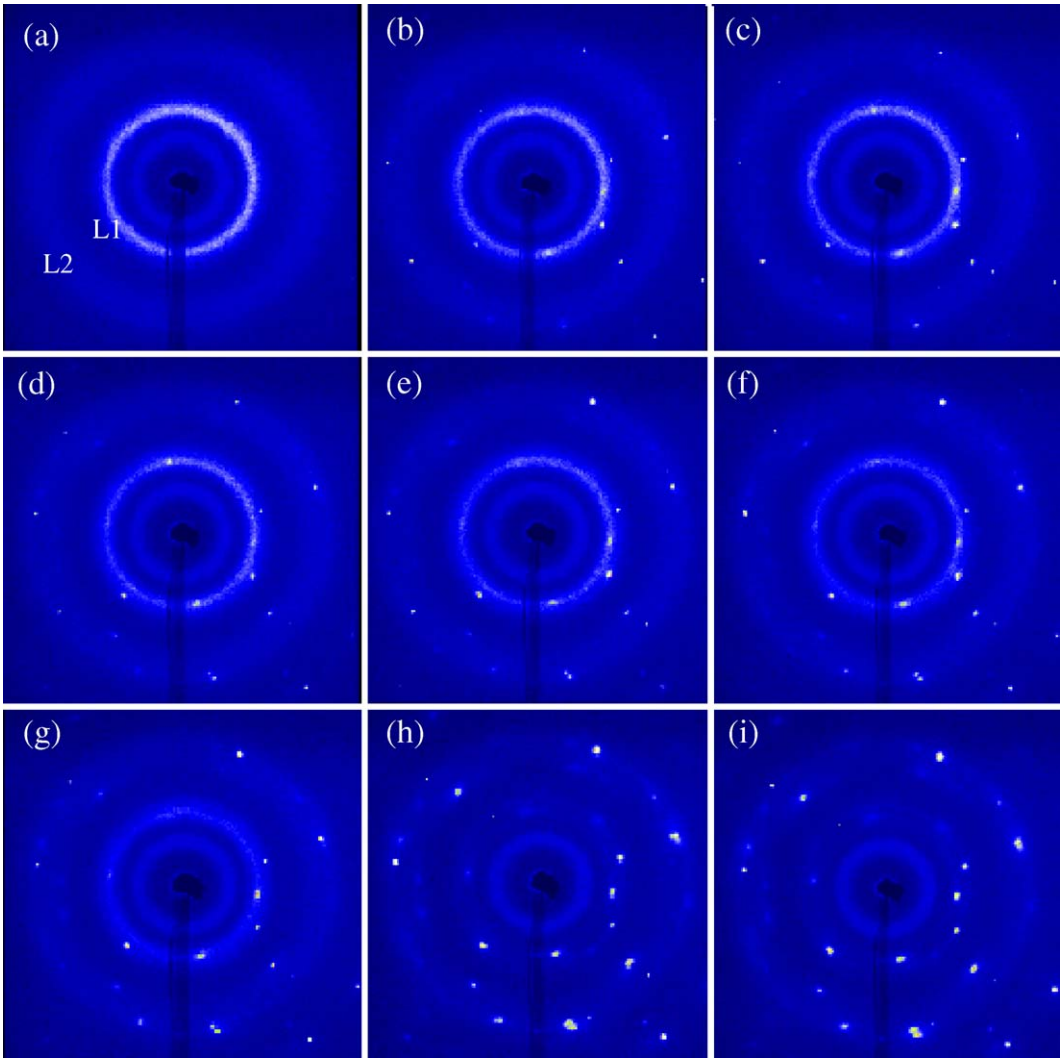

Fig. 10. The X-ray diffraction patterns measured for the Al–0.1Ti–0.1TiB_2 alloy showing the liquid (a) to solid (i) phase transformation during continuous cooling at a cooling rate of 20 K/min. The two broad outer rings L1 and L2 in (a) correspond to the first and second peaks in the liquid structure factor of liquid aluminum, just before solidification. The inner most ring with constant intensity during phase transformation is due to the diffuse scattering from the glassy structure of the sample container. The bright spots are caused by the diffraction from individual grains that nucleate in the early stage of the phase transformation in (b) and grow in number and intensity as the phase transformation proceeds, as shown in figures from (b) to (h). The liquid to solid phase transformation is virtually complete, when no intensity is left in the liquid rings, as shown in figure (i).

Al–0.1Ti–0.1TiB_2 and Al–0.3Ti–0.02B alloys at different cooling rates is presented in Figs. 11–14, respectively. Clearly the undercooling increases for increasing cooling rates. A quantitative comparison of the experimental curves shows that, the nucleation rate during solidification is enhanced only when both solute titanium and TiB_2 particles are present in the melt, as observed in the Al–0.1Ti–0.1TiB_2 and Al–0.3Ti–0.02B alloys. This illustrates the higher nucleation efficiency of TiB_2 particles during solidification, in the presence of solute titanium as predicted by grain refinement theories [1,2]. As reported earlier [9], the nucleation process for almost all the samples investigated, and the applied cooling rates, is always complete for the solid fraction $f_S \approx 0.2$. As shown for the DTA measurements, the growth of nucleated grains leads to a significant release of latent heat [5]. This limits the undercooling ΔT required to activate further nucleation events as the transformation proceeds. The overall nucleation rate is an exponential function of Gibbs free energy, Δg, which is proportional to ΔT [13]. This indicates that a decrease in undercooling caused by the release of latent heat can have striking effects to cease the nucleation process, as observed in Figs. 11–14.

4.2.2. Grain growth versus cooling rate

The growth behaviour of individual aluminum grains during solidification is determined by monitoring the intensity of the diffraction spots during solidification. Fig. 15 illustrates the overall growth kinetics of the individual aluminium grains, for the alloys containing solute titanium with and without added TiB_2 particles. The individual growth curves show a close resemblance to the behaviour of the solid fraction. The observed growth behavior of the individual grains is controlled by the diffusion of solute titanium from the liquid alloy into the solid

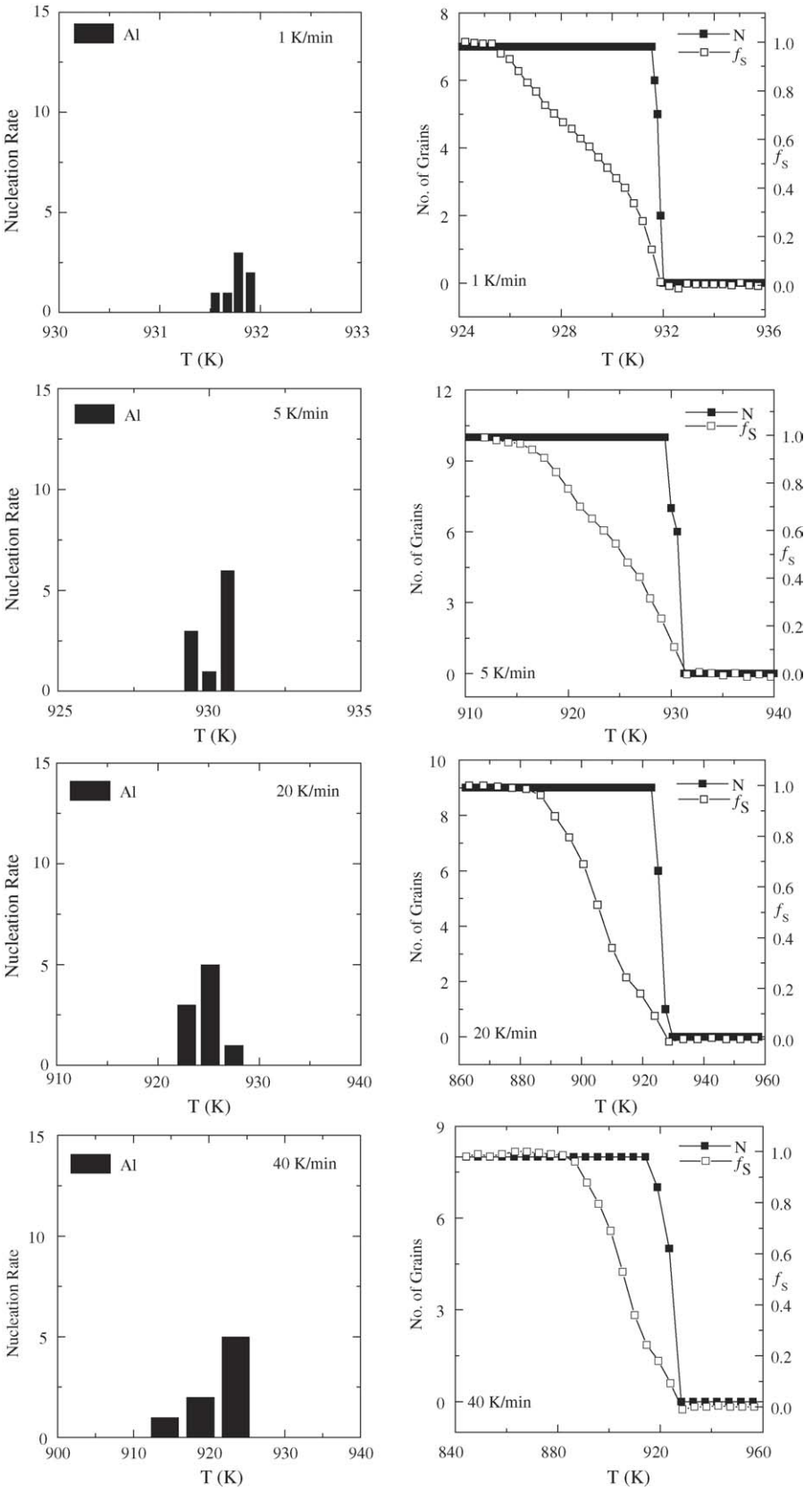

Fig. 11. Nucleation rate, the number of α-aluminum grains (N) and the corresponding evolution of solid fraction (f_S) as a function of temperature during solidification in the Al–0.15TiB_2 (wt.%) alloys at different cooling rates.

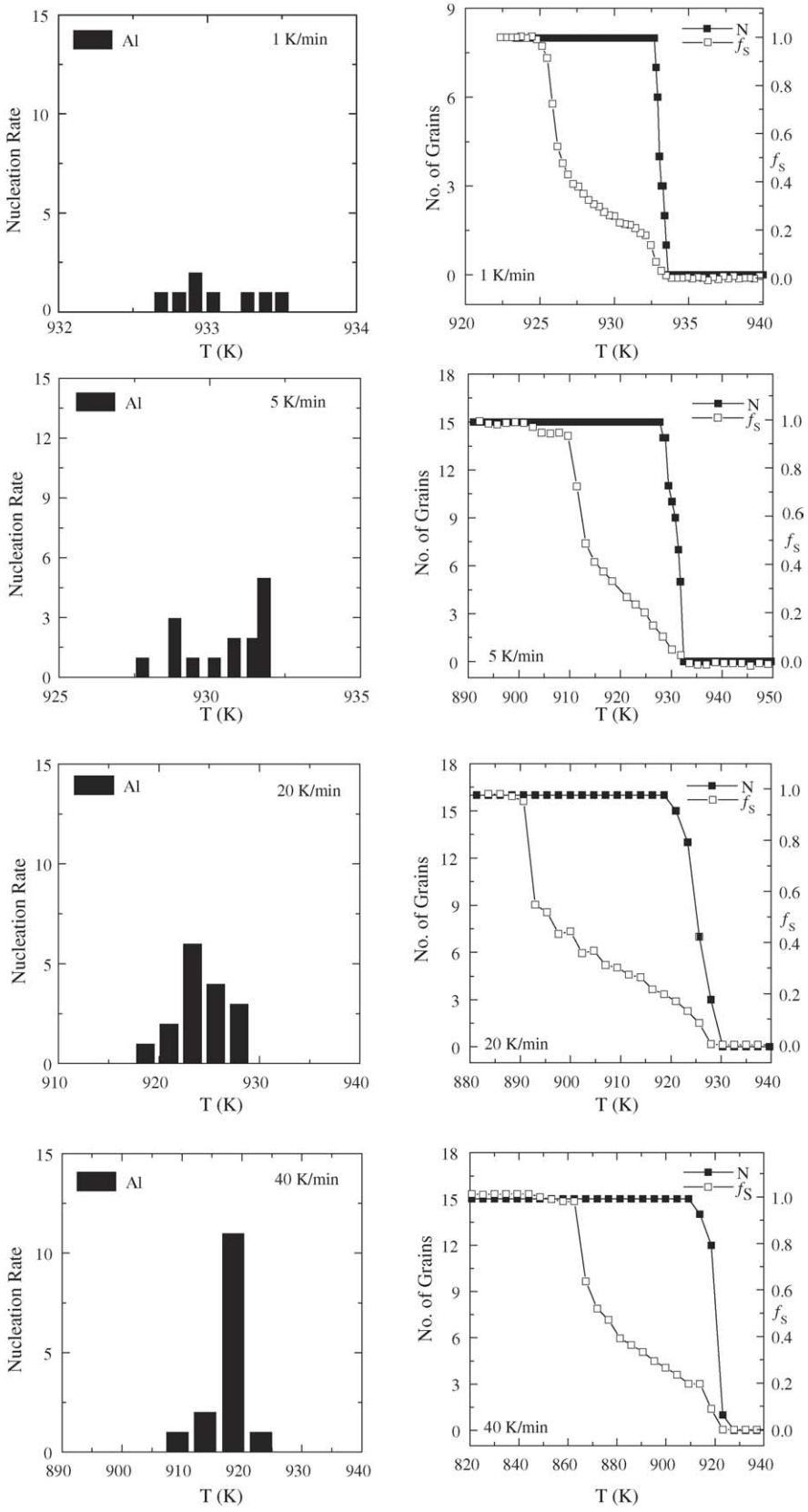

Fig. 12. Nucleation rate, the number of α-aluminum grains (N) and the corresponding evolution of solid fraction (f_S) as a function of temperature during solidification in the Al–0.1Ti (wt.%) alloys at different cooling rates.

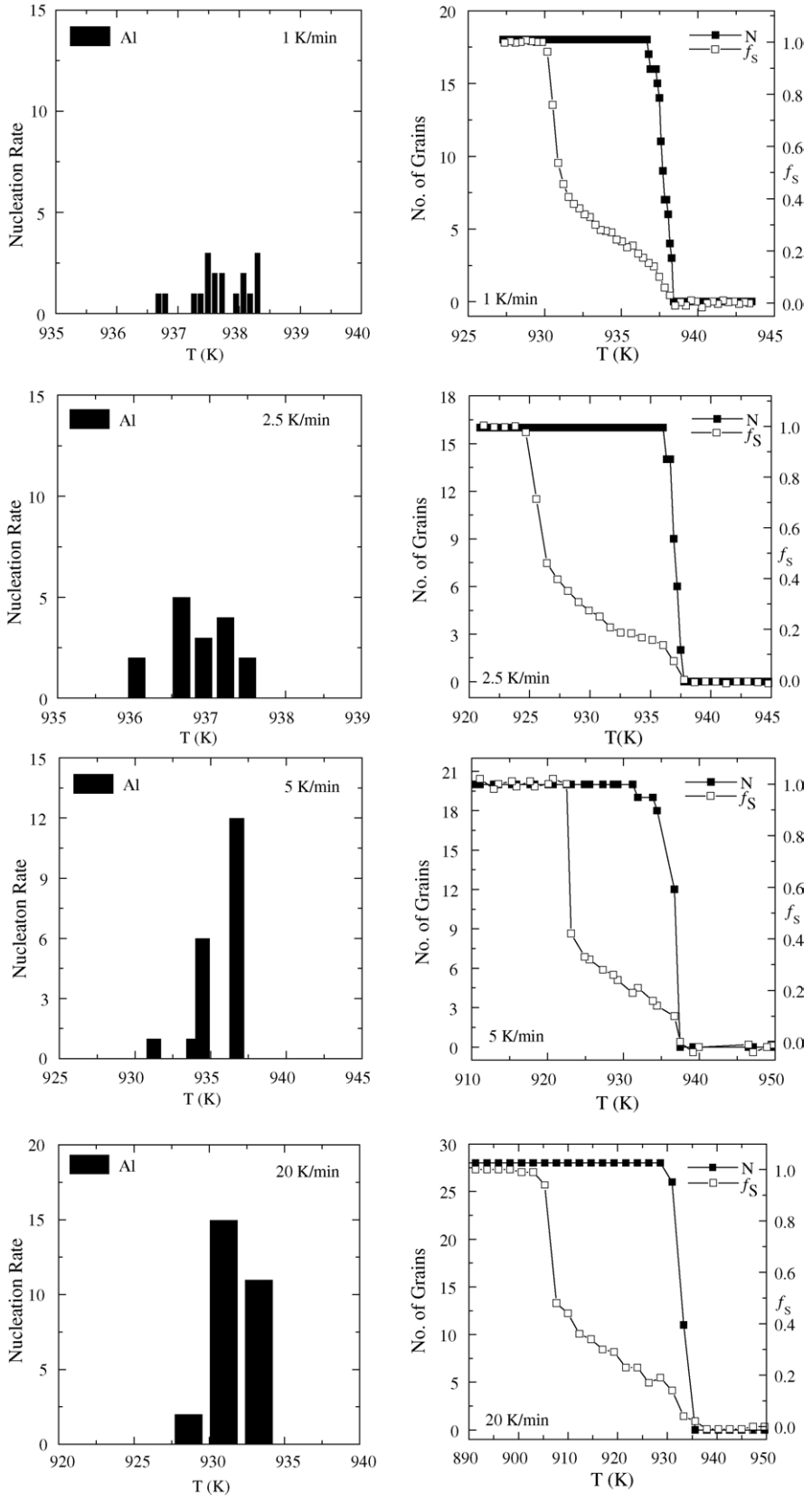

Fig. 13. The nucleation rate, the number of α-aluminum grains (N) and the corresponding evolution of solid fraction (f_S) as a function of temperature during solidification in the Al–0.1Ti–0.1TiB_2 (wt.%) alloys at different cooling rates.

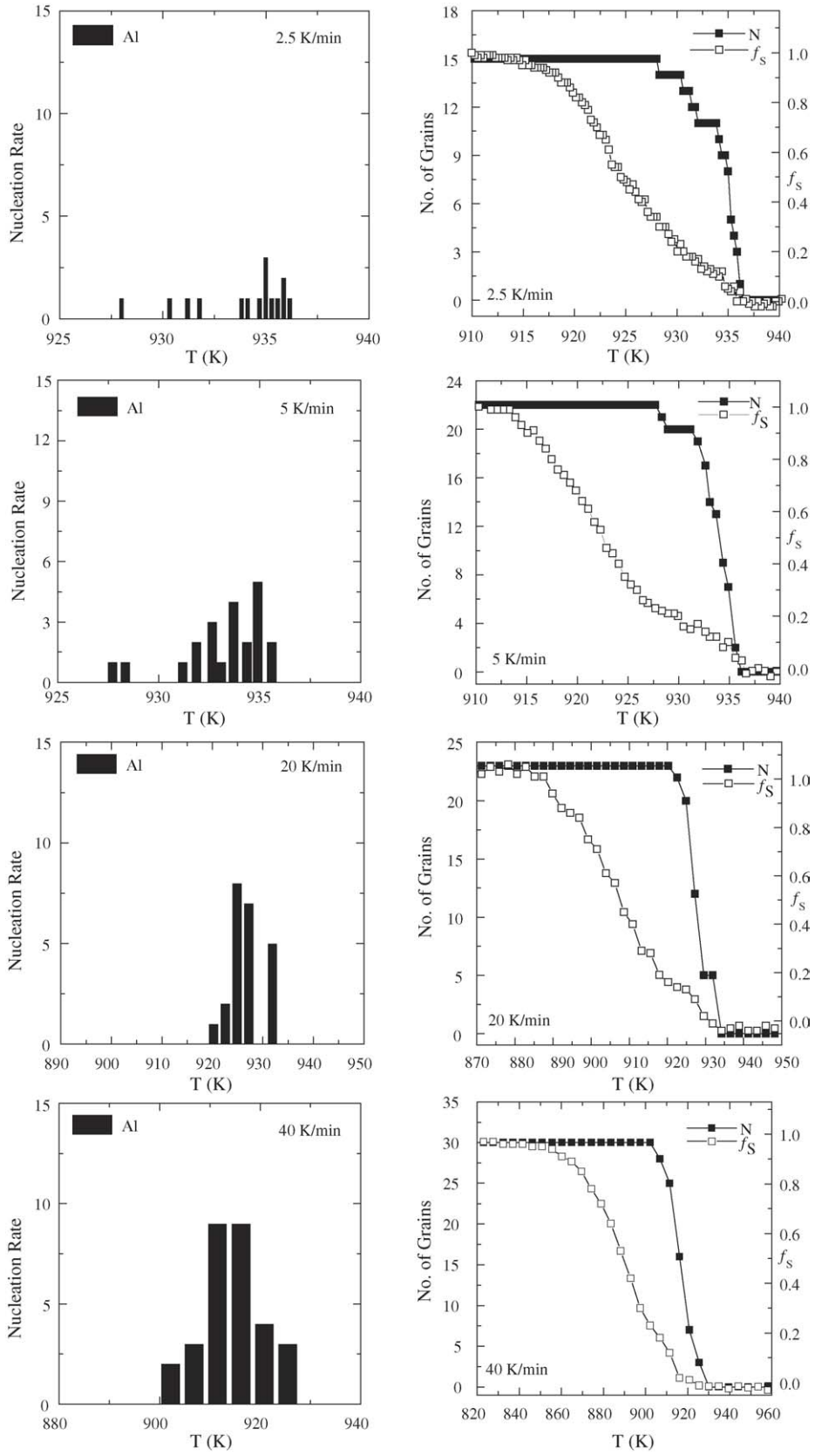

Fig. 14. Nucleation rate, the evolution of α-aluminum grains (N) and the corresponding solid fraction (f_S) as a function of temperature during solidification in the Al–0.3Ti–0.02B (wt.%) alloys at different cooling rates.

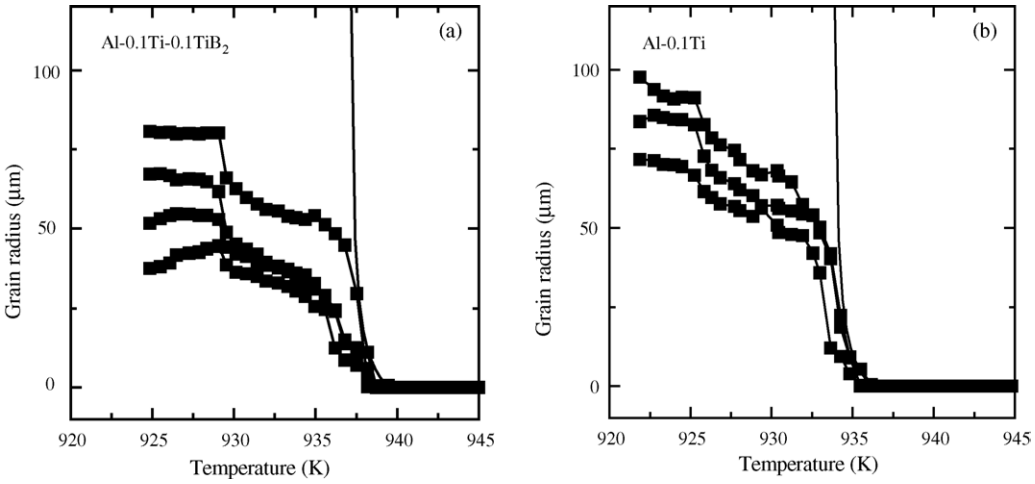

Fig. 15. Grain radius of individual aluminum grains (■) during solidification of Al–0.1Ti–0.1TiB_2 and Al–0.1Ti alloys, as a function of temperature, for continuous cooling at a cooling rate of 1 K/min. The solid lines indicate the model calculation for diffusion-controlled grain growth (from Ref. [9]).

grain. For diffusion-controlled growth the grain radius R as a function of time t is given by [14]:

$$R(t) = \lambda_s \sqrt{D_s(t - t_s)}, \quad (2)$$

where λ_s is a parameter that is determined from the titanium solubility in the liquid and the solid phases, D_s the diffusion constant of solute titanium in the liquid [15] and t_s is the moment of nucleation of the grain. Eq. (2) only applies in the initial stage of the transformation where the interaction between growing grains can be neglected. This is shown in Fig. 15 where the individual growth curves overlap with the model prediction in the initial stage of the transformation. During the later stages the release of latent heat and the interaction of growing grains, reduces the growth.

Fig. 16 shows the growth behaviour of several individual aluminum grains during solidification of the Al–0.1Ti–0.1TiB_2 alloy at cooling rates of 2.5, 5 and 10 K/min. The model prediction for diffusion controlled grain growth is also shown. The observed growth behaviour of individual aluminum grains is similar for all the cooling rates. Again, three different stages for grain growth can be distinguished. The model calculations are in reasonable agreement with the experimental data at slow cooling rates. For higher cooling rates, an increasing undercooling is observed before the nucleation starts. However, the initial growth behaviour exhibits a close resemblance with the model predictions even at higher cooling rates.

4.2.3. Evolution of metastable $TiAl_3$

A careful analysis of the measured diffraction patterns shows the presence of a limited number of weak diffraction spots, prior to the nucleation of aluminum grains, during slow cooling of the liquid Al–0.1Ti–0.1TiB_2 and Al–0.3Ti–0.02B alloys. These diffraction spots cannot be indexed as aluminium grains. The crystallographic analysis indicates that the scattering angles corresponding to these diffraction spots fit to the $TiAl_3$ phase with two different crystallographic structures, tetragonal as well as cubic. Figs. 17 and 18 describe the evolution of these $TiAl_3$ grains during continuous cooling of the liquid Al–0.1Ti–0.1TiB_2 and Al–0.3Ti–0.02B alloys at slow cooling rates. It is interesting to see that these diffraction spots first appear roughly 10 K above the experimental solidification temperature of aluminum. At the nucleation temperature of the aluminum grains the intensity of the $TiAl_3$ reflections start to decrease, and finally vanish near the end of the transformation. The absence of these $TiAl_3$ reflections in the sample containing only solute titanium or only TiB_2 particles shows that the $TiAl_3$ phase plays an essential role in the enhanced nucleation process as revealed in Figs. 13 and 14, compared to that observed in Figs. 11 and 12. This formation of $TiAl_3$ phases prior to the nucleation of aluminium grains in Al–0.1Ti–0.1TiB_2 and Al–0.3Ti–0.02B alloys favours our interpretation of the crystallization process during the DTA measurements of these samples. Apparently, the nucleation of $TiAl_3$ on the TiB_2 substrate is substantially more effective than the nucleation of aluminum. From earlier measurements it is known that once $TiAl_3$ is formed it acts as an excellent nucleation site for aluminum [16]. Our present in situ study shows that the TiB_2 substrates stabilise a $TiAl_3$ phase in a limited temperature range above the solidification temperature of aluminum. This formation of a $TiAl_3$ phase in aluminum alloys with a titanium concentration below 0.15 wt.%, where it is considered unstable according to the Al–Ti phase diagram [17], has long been proposed but was so far not supported by experimental evidence due to the lack of in situ data [2,11].

While according to the Al–Ti phase diagram, the $TiAl_3$ is a stable phase in an hyperperitectic aluminum alloy, above the melting temperature. Our measurements indicate that upon nucleation of α-aluminum grains during continuous cooling, the $TiAl_3$ grains cease to grow and their radius decreases with a further decrease in temperature of both hyperperitectic and hypoperitectic grain refined aluminium alloys. No such observation of the evolution of a $TiAl_3$ phase within the melt has been reported earlier.

The role played by the $TiAl_3$ phase in the nucleation of α-aluminum during solidification of grain refined aluminum alloys has been a matter of speculations. The $TiAl_3$ substrate is con-

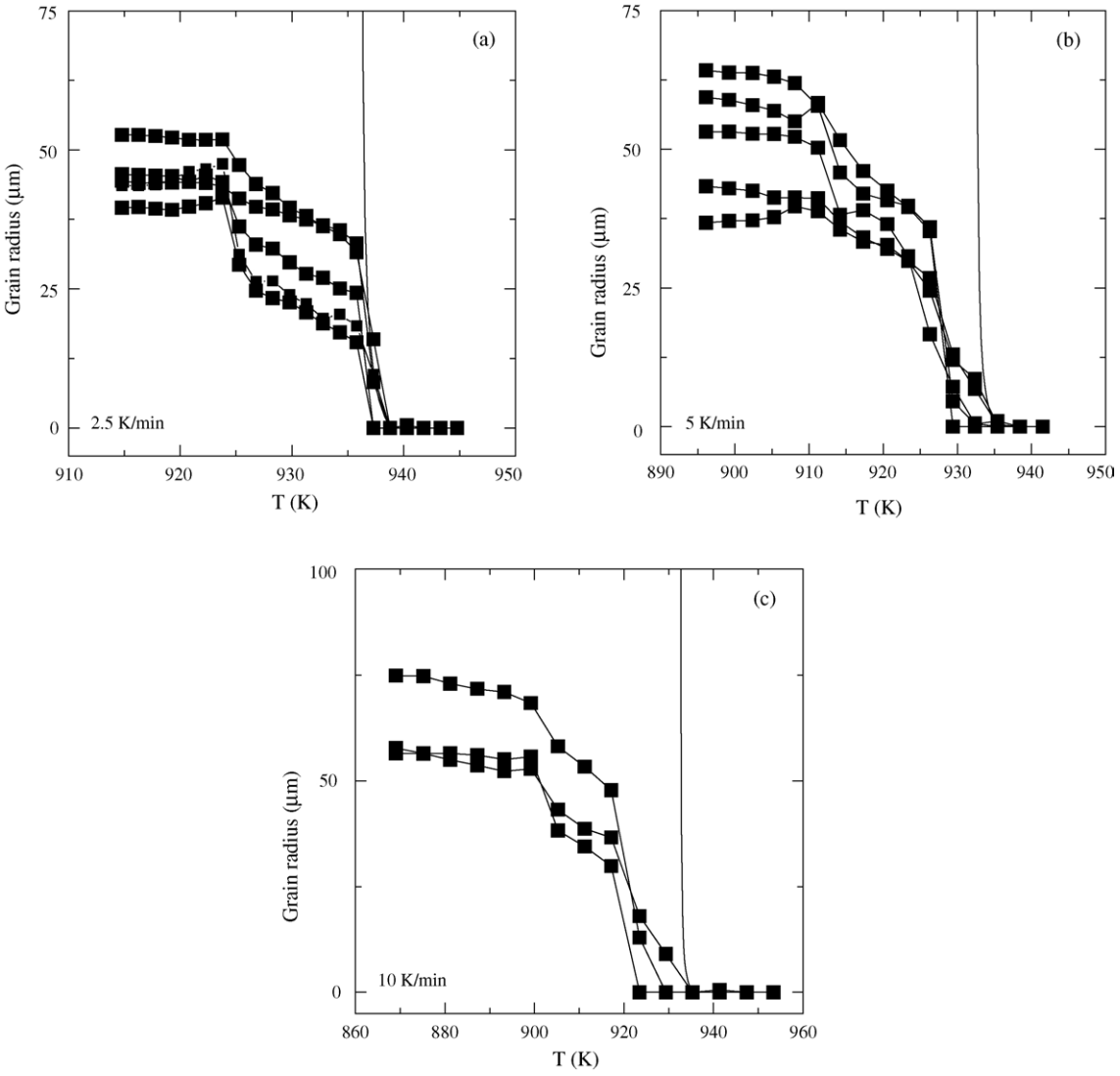

Fig. 16. Grain radius of individual aluminum grains (■) during solidification of Al–0.1Ti–0.1TiB_2 alloy, as a function of temperature, with continuous cooling at different cooling rate (a) 2.5 K/min, (b) 5 K/min, and (c) 10 K/min. The solid lines indicate the model calculation for diffusion-controlled grain growth.

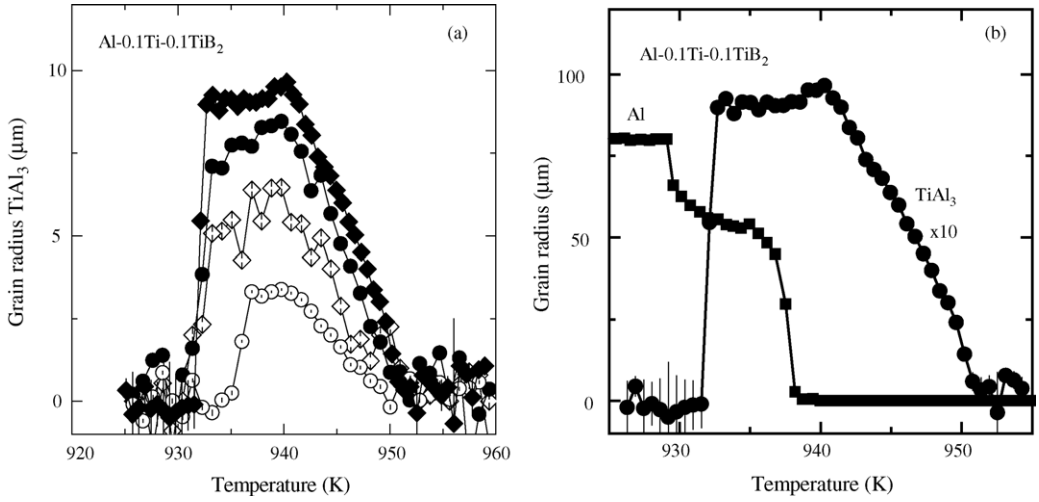

Fig. 17. The grain radius of individual $TiAl_3$ grains in the aluminium alloy with solute titanium and added TiB_2 particles (a) and compared to the growth of an individual aluminium grain in (b). The $TiAl_3$ grains nucleate about 10 K above the experimental onset of nucleataion for aluminium grains, and become unstable when solid aluminium has formed (from Ref. [9]).

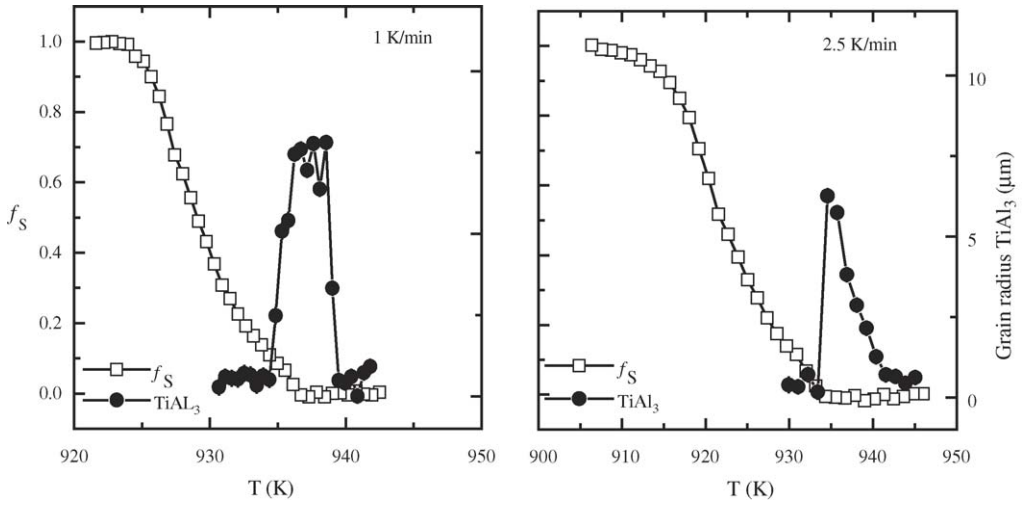

Fig. 18. Evolution of the solid fraction f_S of aluminum (□) and the radius of $TiAl_3$ grains (●) during liquid to solid phase transformation of the Al–0.3Ti–0.02B alloy at a slow cooling rate of 1 and 2.5 K/min. The solid fraction of aluminum is deduced from the normalized variation in the intensity of the first liquid peak of aluminum.

sidered to be a better nucleation site for aluminum grains than the TiB_2 particles, and hence, responsible for grain refinement. Previously Mohanty et al. have confirmed this mechanism and reported the existence of $TiAl_3$ layer sandwiched between the TiB_2 surface and the aluminum grains, in grain refined aluminum alloys. Our experimental observations support those reported by Mohanty et al. It suggests that the surface of TiB_2 particles, nucleate $TiAl_3$ grains prior to the solidification of aluminum. However these $TiAl_3$ grains exhibit a metastable behavior. The $TiAl_3$ grains dissolve upon solidification of aluminum and most probably responsible for the enhanced nucleation of aluminum grains.

5. Conclusions

We have performed DTA and 3D XRD measurements to study the crystallization kinetics and mechanism of grain nucleation and growth of individual grains during the liquid to solid phase transformation of grain refined aluminum alloys. The formation of a $TiAl_3$ phase is observed to be responsible for enhanced nucleation in hyperperitectic, as well as hypoperitectic grain refined aluminium alloys. The growth behaviour of individual aluminium grains, just after nucleation, is controlled by titanium diffusion. However, afterwards the release of latent heat is also crucial in governing the growth kinetics during solidification.

Acknowledgements

We are grateful to L. Zhao for assistance with the thermodynamical calculations using MTDATA. We acknowledge the European Synchrotron Radiation Facility for provision of synchrotron radiation facilities and we would like to thank G. Vaughan and A. Götz for assistance in using beamline ID11. This work was financed in part by The Netherlands Foundation for Fundamental Research of Matter (FOM) and the Netherlands Institute for Metals Research (NIMR).

References

[1] M. Easton, D. Stjohn, Met. Mater. Trans. A 30 (1999) 1613.
[2] M. Easton, D. Stjohn, Met. Mater. Trans. A 30 (1999) 1625.
[3] A. Cibula, J. Inst. Met. 80 (1951) 1.
[4] A. Marcantonio, L.F. Mondolfo, Met. Trans. 2 (1971) 465.
[5] I. Maxwell, A. Hellawell, Acta Met. 23 (1975) 229.
[6] L. Backerud, Light Met. Age. 41 (1983) 6.
[7] G.K. Sigworth, Met. Trans. A 15 (1984) 277.
[8] A.L. Greer, A.M. Bunn, A. Tronche, P.V. Evans, D. Bristow, J. Acta Mater. 48 (2000) 2823.
[9] N. Iqbal, N.H. van Dijk, S.E. Offerman, M.P. Moret, L. Katgerman, G.J. Kearley, Acta Mater. 53 (2005) 2875.
[10] N. Iqbal, N.H. van Dijk, S.E. Offerman, M.P. Moret, L. Katgerman, G.J. Kearley, Mater. Res. Soc. Symp. Proc., Boston, USA 840 (2005) Q7.12.
[11] P.S. Mohanty, J.E. Gruzleski, Acta. Metall. Mater. 43 (1995) 2001.
[12] P. Schumacher, A.L. Greer, Mater. Sci. Eng. A 178 (1994) 309.
[13] W. Kurz, D.J. Fisher, Fundamentals of Solidification, Trans Tech Publications Ltd, Switzerland, 1998.
[14] C. Zener, J. Appl. Phys. 20 (1949) 950.
[15] G.S. Ershov, A.A. Kasatkin, A.A. Golubev, Russian Metall. 2 (1978) 62.
[16] A.L. Greer, Phil. Trans. R. Soc., Lond. A 361 (2003) 479.
[17] D.G. McCartney, Int. Mater. Rev. 34 (1989) 247.
[18] M.V.J. Quaresma, A.C. Santos, M. Garcia, Met. Mater. Trans. A 31 (2000) 3167.